

## DETECTION OF BIPOLAR FLOW TOWARD THE UNUSUAL SiO MASER SOURCE IRAS 19312+1950

JUN-ICHI NAKASHIMA<sup>1</sup> AND SHUJI DEGUCHI<sup>2</sup>

Received 2004 March 29; accepted 2004 June 10; published 2004 June 22

### ABSTRACT

We report results of an interferometric observation toward an SiO maser source, IRAS 19312+1950, in the  $\text{HCO}^+ J = 1-0$  line with the Berkeley-Illinois-Maryland Association millimeter array. In the spatially integrated spectrum of  $\text{HCO}^+$ , two kinematic components were seen: a strong line with a narrow width ( $\sim 2 \text{ km s}^{-1}$ , narrow component) and a weak symmetric line with a broad width ( $\sim 60 \text{ km s}^{-1}$ , broad component). The line profile of  $\text{HCO}^+$  is reminiscent of that of CO. In the integrated intensity map, we found a pronounced bipolar shape consisting of the lower velocity part of the broad component. The higher velocity part of the broad component originated in a relatively small region ( $\leq 3''$ ). The spatial structure of the narrow component clearly correlates with near-infrared structure. The position-velocity diagrams indicate the presence of a bipolar outflow with an expansion velocity of about  $10 \text{ km s}^{-1}$ . On the basis of the present results, we suggest that the nature of the bipolar flow seen in IRAS 19312+1950 is explained by the hydrodynamical interaction between an asymptotic giant branch wind and ambient material with axial symmetric structure.

*Subject headings:* circumstellar matter — ISM: jets and outflows — masers — stars: imaging — stars: individual (IRAS 19312+1950) — stars: winds, outflows

### 1. INTRODUCTION

IRAS 19312+1950 is an SiO maser source that was discovered by Nakashima & Deguchi (2000) in their SiO maser surveys toward selected *IRAS* sources in the Galactic plane (Nakashima & Deguchi 2003a, 2003b). Nakashima & Deguchi (2000) first suggested that IRAS 19312+1950 was an asymptotic giant branch (AGB)/post-AGB star that evolved from a relatively massive progenitor on the basis of its prominent bipolar shape seen in near-infrared images and the low color temperature of the dust envelope. In fact, SiO maser sources are usually identified as late-type stars with active mass loss. Subsequently, they have found two remarkable characteristics of this object: (1) two kinematic components in molecular line profiles (a strong line with a narrow width of  $\leq 2 \text{ km s}^{-1}$  and a weak-symmetric line with a broad width of  $\geq 60 \text{ km s}^{-1}$ ; Nakashima et al. 2004) and (2) a rich set of molecular species (Nakashima et al. 2004; Deguchi & Nakashima 2003). In addition, recent near-infrared observations (K. Murakawa 2004, in private communication) suggested that there is a ringlike structure with a size of about  $10''$  around the central star. Some of the characteristics found in IRAS 19312+1950 are often seen in dark clouds (or young stellar objects [YSOs]). However, secure examples of YSOs emitting SiO masers are quite limited; actually, there are only three: Ori IRc 2, W51 IRs 2, and Sgr B2 MD5 (see, e.g., Hasegawa et al. 1986). These YSOs with SiO masers lie in the extreme star-forming regions (in giant molecular clouds), which are clearly identified as largely extended nebulae in infrared images, whereas no clear star-forming activity is seen around IRAS 19312+1950 in infrared images. Thus, the evolutionary status of IRAS 19312+1950 is not yet definitely known.

To investigate the nature of this highly unusual SiO maser source, we are currently conducting high spatial resolution interferometric observations using the Berkeley-Illinois-Maryland Association (BIMA) array in several molecular rotational lines detected by our single-dish observations (Nakashima &

Deguchi 2000; Nakashima et al. 2004; Deguchi & Nakashima 2003). In this Letter, we report the first results of the interferometric observations in the  $\text{HCO}^+ J = 1-0$  line and the detection of a bipolar flow, which might be interpreted as an interaction between an AGB wind and ambient material.

### 2. OBSERVATION AND RESULTS

Interferometric observations of IRAS 19312+1950 were made with the BIMA millimeter array from 2003 December to 2004 January. The instrument is described in detail by Welch et al. (1996). We observed the  $\text{HCO}^+ J = 1-0$  line at 89.188526 GHz with the BIMA array, consisting of 10 elements in one configuration (B array). The observations were interleaved every 25 minutes with the nearby point source, 1925+211, to track the phase variations over time. The absolute flux calibration was determined from observations of Uranus and is accurate to within 20%. The final map has an accumulated on-source observing time of about 15 hr. Typical single-sideband system temperatures ranged from 200 to 300 K. The velocity coverage was  $380 \text{ km s}^{-1}$ , using three different correlator windows with a bandwidth of 50 MHz each. The velocity resolution was  $1.3 \text{ km s}^{-1}$ . The phase center of the map was R.A. =  $19^{\text{h}}33^{\text{m}}24^{\text{s}}.4$ , decl. =  $19^{\circ}56'54''.8$  (J2000) corresponding to the *IRAS* position of this object. Data reduction was performed with the MIRIAD software package (Sault et al. 1995). Standard data reduction, calibration, imaging, and deconvolution procedures were followed. Robust weighting of the visibility data gave a  $3''.7 \times 2''.5$  CLEAN beam with a position angle of  $23^\circ$ . The rms noise per  $1.0 \text{ km s}^{-1}$  is  $3.8 \times 10^{-2} \text{ Jy beam}^{-1}$ .

Figure 1 shows the spectrum of the  $\text{HCO}^+ J = 1-0$  line. A remarkable feature of the spectrum is the strong line with a narrow width ( $\sim 2 \text{ km s}^{-1}$ ) peaked at  $V_{\text{LSR}} \sim 38 \text{ km s}^{-1}$ . A weak symmetric line with a broad width ( $\sim 60 \text{ km s}^{-1}$ ) is also seen in the velocity range of  $V_{\text{LSR}} \sim -10$  to  $70 \text{ km s}^{-1}$ . For convenience, we call the former the “narrow component” and the latter the “broad component.” The narrow component is roughly centered on the broad component. Absorption features are seen beside the narrow component, suggesting that cold gas components lie in the foreground. The line profile of  $\text{HCO}^+$  is reminiscent of that of the CO  $J = 1-0$  (and  $J = 2-1$ ) line

<sup>1</sup> Department of Astronomy, University of Illinois at Urbana-Champaign, 1002 West Green Street, Urbana, IL 61801; junichi@astro.uiuc.edu.

<sup>2</sup> Nobeyama Radio Observatory, National Astronomical Observatory, Minamimaki, Minamisaku, Nagano 384-1305, Japan; deguchi@nro.nao.ac.jp.

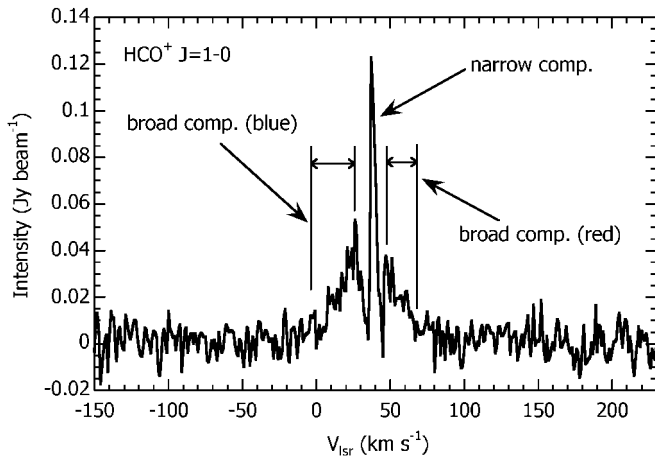


FIG. 1.—Spatially integrated spectrum of IRAS 19312+1950 in the  $\text{HCO}^+$   $J = 1-0$  line. The integrated area is a circle with a diameter of  $15''$ . The vertical solid lines represent the velocity ranges of the blue- and redshifted wings of the broad component used for Fig. 2.

(see, e.g., Nakashima et al. 2004). Similar line profiles, including the two kinematic components (narrow and broad components), have been reported in some AGB stars (e.g., EP Aqr, X Her, and RV Boo; Kahane & Jura 1996; Kerschbaum & Olofsson 1999; Knapp et al. 1998). Kahane & Jura (1996) reported on a bipolar flow consisting of the broad component seen in X Her, and Knapp et al. (1998) suggested a scenario in which episodic mass loss plays a role in explaining the kinematic components seen in these AGB stars. Figure 2 shows velocity-integrated intensity maps in three different velocity ranges corresponding to the narrow component (*dashed contours*) and the blue- and redshifted wings of the broad component (*thin and thick solid contours, respectively*). The map is superposed on a combined near-infrared image ( $J$ ,  $H$ , and  $K$  bands) taken by the CIAO (Coronagraphic Imager with Adaptive Optics) camera on the Subaru telescope (courtesy of K. Murakawa, M. Tamura, and the CIAO group of the National Astronomical Observatory in Japan). The velocity ranges used for computing integrated intensities are indicated in Figure 1 and in the caption of Figure 2. The source is clearly resolved by the synthesized beam (shown at the lower right in Fig. 2). Although we observed with only one configuration, most of the flux emitted from the source is thought to be detected according to the upper limit of the source size ( $\sim 30''$ ) determined by our single-dish observation (Nakashima et al. 2004). As the most pronounced feature in the map, we can see a bipolar shape consisting of the thin and thick contours. The apparent axis of the bipolar shape is close to the north-northeast–south-southwest direction. If the bipolar shape originates in a bipolar outflow, the lower side (southern component) should be closer to us, and the upper side (northern component) should be farther from us. Interestingly, the structure of the blueshifted wing (*thin contours*) of the broad component shows two extended tails: the strong tail to the southeast and the weak tail to the east (exhibiting a “lying-Y” shape). The structure of the redshifted wing (*thick contours*) extends only to the northeast. On the contrary, the structure of the narrow component (*dashed contours*) is somewhat more complicated. Three intensity peaks are seen in the dashed contours at the points of  $3''$ ,  $4''$ , and  $8''$  from the map center to the northeast, northwest, and east, respectively. Although the positions of these peaks of the narrow component do not correspond to the bright regions seen in the near-infrared image (background of Fig. 2), it looks as though

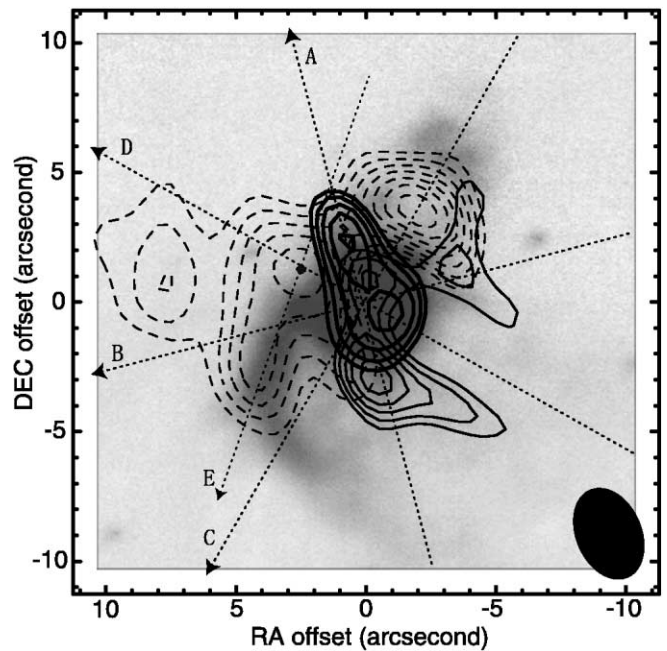


FIG. 2.— $\text{HCO}^+$ -integrated intensity map (*contours*) superposed on a near-infrared composite ( $J$ ,  $H$ , and  $K$  bands) image (*gray scale*) taken by the Subaru telescope. The ranges of velocity integration for the thick, thin, and dashed contour maps are  $0-26$ ,  $47-60$ , and  $37-38$   $\text{km s}^{-1}$ , respectively. The contour levels start from a  $5\sigma$  level and increase every  $0.5\sigma$  for the broad component and every  $1\sigma$  for the narrow component. The  $1\sigma$  levels of the thin, thick, and dashed contour maps are  $7.3 \times 10^{-3}$ ,  $1.0 \times 10^{-2}$ , and  $2.7 \times 10^{-2}$   $\text{Jy beam}^{-1}$ , respectively. The synthesized beam is indicated in the lower right-hand corner. The dotted arrows (A, B, C, D, and E) denote “cuts” used for the  $p$ - $v$  diagrams in Fig. 3. The filled circle represents the origin of cut E.

the global structure of the narrow component clearly correlates with the near-infrared structure. From the apparent size of the  $\text{HCO}^+$  structure and the assumption of the density, we can crudely estimate the mass of the source. If we assume that the source is a homogeneous sphere with a diameter of  $10''$ , the mass is estimated to be  $4-31 M_{\odot}$ ; we used the distance ( $2.5-5.1$  kpc) estimated by Nakashima et al. (2004) and the assumed density of  $10^4 \text{ cm}^{-3}$  traced by the  $\text{HCO}^+$  line.

To investigate the kinematic structure, we made position-velocity ( $p$ - $v$ ) diagrams at various cuts. Figure 3 shows the  $p$ - $v$  diagrams at selected cuts. In the top four diagrams in Figure 3, velocity channels are averaged over  $2 \text{ km s}^{-1}$  intervals. The cuts used for the diagrams are indicated in Figure 2 as the dotted arrows. The directions of the arrows in Figure 2 represent the positive direction of the offset axes in Figure 3. The origins of the cuts A, B, C, and D are taken at the phase center. The origin of cut E is indicated by the filled circle in Figure 2. Cut “A” corresponds to the apparent axis of the bipolar shape. Cut “B” represents the perpendicular cut to cut A. Cut “C” corresponds to the major axis of the ringlike structure seen in near-infrared images. Cut “D” represents the perpendicular cut to cut C. Cut “E” is mentioned later. Although the global structure seen in Figure 3 is highly clumpy, the spatial size (vertical size of structure) of the source tends to be smaller in higher velocity regions. The intensity peaks lie nearly on the origins of vertical axes in velocity ranges  $V_{\text{LSR}} \lesssim 20 \text{ km s}^{-1}$  and  $V_{\text{LSR}} \gtrsim 50 \text{ km s}^{-1}$ . In addition, maximum velocity widths (represented by the maximum widths of the lowest contours in the horizontal coordinates) do not exhibit any noticeable variations with respect to the position angle. These facts mean that the higher velocity part ( $|V_{\text{LSR}} - V_{\text{sys}}| \gtrsim 15 \text{ km s}^{-1}$ ; here, we assume that the system

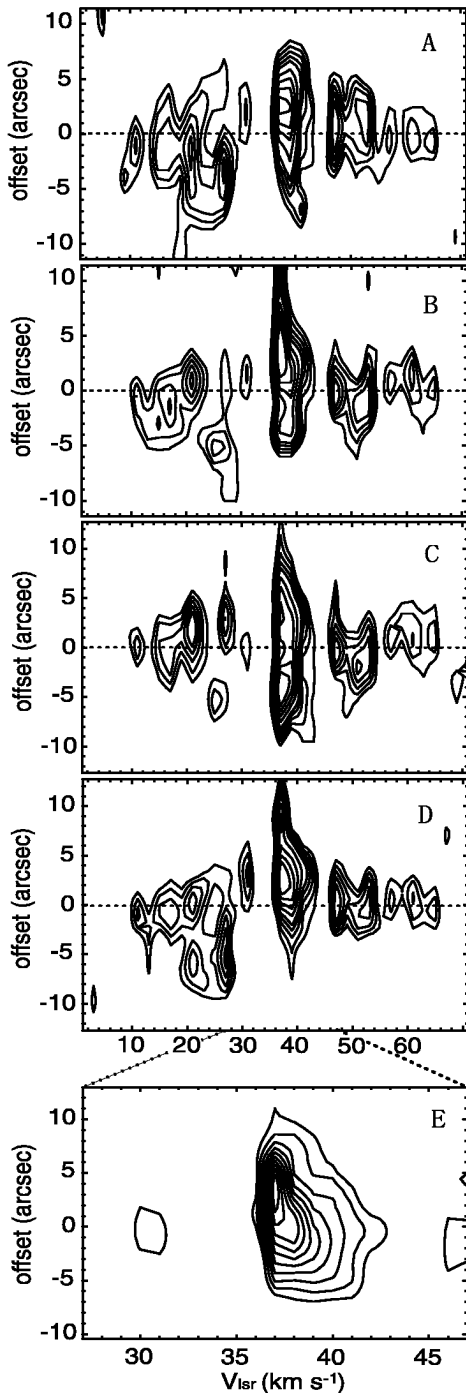


FIG. 3.—Position-velocity diagrams along the cuts indicated in Fig. 2. The velocity channels are averaged over 2 km s<sup>-1</sup> intervals, except for the bottom panel. In the top four diagrams, the contours are drawn from 40 mJy beam<sup>-1</sup> with increments of 10 mJy beam<sup>-1</sup> between 40 and 80 mJy beam<sup>-1</sup> and 20 mJy beam<sup>-1</sup> between 80 and 160 mJy beam<sup>-1</sup>. The bottom panel is the  $p$ - $v$  diagram along cut E without velocity channel binding. In the bottom panel, the contours start from 60 mJy beam<sup>-1</sup> with increments of 20 mJy beam<sup>-1</sup>.

velocity is  $V_{\text{sys}} \sim 37$  km s<sup>-1</sup>) of the broad component is not resolved by our synthesized beam and should originate in a relatively small region ( $\lesssim 3''$ ). On the other hand, variations of structure are found in the lower velocity ranges ( $|V_{\text{LSR}} - V_{\text{sys}}| \lesssim 15$  km s<sup>-1</sup>) of the broad component, especially on the blueshifted side ( $20$  km s<sup>-1</sup>  $\lesssim V_{\text{LSR}} \lesssim 35$  km s<sup>-1</sup>). In fact, intensity peaks at  $V_{\text{LSR}} \sim 25$ – $27$  km s<sup>-1</sup> clearly shift to the negative direction in the offset axes. These peaks correspond to the south-

ern and northern tails of the blueshifted wing (see thin contours in Fig. 2). The 27 km s<sup>-1</sup> peaks seen in the cuts A, C, and D correspond to the southern tail, and the 25 km s<sup>-1</sup> peak seen in cut B corresponds to the northern tail. On the contrary, in the redshifted side, no clear variations of structure are seen except for an extension to the positive direction in the offset axis in cut A (and possibly in C) at  $V_{\text{LSR}} \sim 47$  km s<sup>-1</sup>. We also made  $p$ - $v$  diagrams without channel binding to check the motion of the narrow component in several cuts. Finally, we found the most pronounced variation of structure in cut E corresponding to the tail growing to the southeast from the intensity peak at (decl., R.A.)<sub>offset</sub> = (1'1, -2'5). The  $p$ - $v$  diagram in cut E is shown in the bottom panel of Figure 3, and there is a clear variation of structure as a function of radial velocity. The peak has another tail extended to the southwest. The southwest tail also exhibits a systematic variation of structure in a  $p$ - $v$  diagram, although the diagram is not shown in this Letter. In any other cuts, no clear variation of velocity structure is found in the narrow component. We are likely to see complicated variations of the narrow component in the top four panels of Figure 3. These structures are explained well by a superposition of the two flows mentioned above.

### 3. DISCUSSION

The bipolar flow seen in IRAS 19312+1950 consists of the lower velocity part of the broad component, whereas the higher velocity part originates in a small region with a size of less than about 3''. Usually, the expansion velocity of bipolar flows seen in late-type stars (especially in post-AGB stars) tends to increase with distance from the central star (frequently called a "Hubble-type flow" in this area; see Balick & Frank 2002); the nature of the bipolar flow seen in IRAS 19312+1950 is in disagreement with this point. In our opinion, the characteristics of the bipolar flow are explained by the hydrodynamical interaction between a spherical outflow lying at the center and the ambient material with axial symmetric structure, if the spherical outflow expelled from the central star is distorted to a bipolar shape by the interaction. In such a case, the slow expanding velocity of the bipolar flow seems to be somewhat strange, but the slow velocity would be explained by a projection effect if the flow has an inclination angle of 20° (where we assume the velocity of the bipolar flow equals a half of the maximum width of the broad component, i.e.,  $\sim 30$  km s<sup>-1</sup>). Interestingly, in Figure 2, the bipolar shape precisely escapes from dense regions of the narrow component, and the redshifted component of the bipolar flow lies in the interspace between two remarkable intensity peaks of the narrow component. In addition, the absorption feature beside the narrow component seen in Figure 1 might be explained as the near side of the ambient material (with axial symmetric structure).

If the higher velocity part of the broad component is a spherical outflow from the central star, the flow should be identified as an AGB outflow because the spherical outflow is the typical nature of AGB envelopes and also because the expanding velocity of  $V_{\text{exp}} \sim 30$  km s<sup>-1</sup> is very reasonable, as seen in the superwind phase at the late-AGB stage. Our recent CO data taken by the BIMA array also support the notion that the inner part of the nebulosity is made up of spherical properties. However, one problem is the somewhat strong HCO<sup>+</sup> intensity (especially in the outermost parts of the envelope) if the central star is an O-rich AGB star, because the HCO<sup>+</sup> line is usually weak or null in AGB envelopes, except in a few cases (Nguyen-Q-Rieu et al. 1988; Deguchi et al. 1990; Cox et al. 1992). From

the viewpoint of theory, the  $\text{HCO}^+$  molecule can be produced by a photochemical process in an O-rich AGB envelope up to a radius  $\sim 2 \times 10^{17}$  cm (see, e.g., Mamon et al. 1987, who in their calculation took account of ionization by galactic and stellar UV photons and of high-energy particles). However, we still need additional chemical processes to explain the effective formation of  $\text{HCO}^+$  in the outermost parts of the envelope because it is most likely that the outermost part of  $\text{HCO}^+$  emission is farther than  $10^{17}$  cm from the central star if the central star is an AGB star (with an estimated distance of 2.5–5.1 kpc; see Nakashima et al. 2004). One immediate possibility of explaining the highly extended  $\text{HCO}^+$  structure would be “dissociative shock.” Actually, most AGB envelopes exhibiting the  $\text{HCO}^+$  emission show signs of shock (e.g., Cox et al. 1992). The  $\text{HCO}^+$  emission in OH 231.8+4.2, which is a well-known example of an SiO maser source with a bipolar shape, is also explained by shocks (Sánchez Contreras et al. 2000). Shock ionization also supports our explanation for the kinematic structure of the bipolar flow because shock fronts are likely to be produced between an AGB wind and ambient material.

The remaining problems in the AGB star interpretation are the excess of mass and of the mass-loss rate. Although we estimated the mass to be  $4\text{--}31 M_{\odot}$ , it will be over  $8 M_{\odot}$  if the distance exceeds 3 kpc. In such a case, the nebulosity cannot be explained as material expelled from a central AGB star. If we assume a spherical flow and a density of  $10^4 \text{ cm}^{-3}$  at  $10^{17}$  cm from the central star, the mass-loss rate is estimated to be about  $10^{-4} M_{\odot} \text{ yr}^{-1}$  in terms of the expanding velocity of the broad component ( $\sim 30 \text{ km s}^{-1}$ ). This mass-loss rate is slightly larger than is typical for AGB stars ( $\sim 10^{-5} M_{\odot} \text{ yr}^{-1}$ ). The keys to checking the AGB possibility would be near-star kinematics and the isotope ratio (e.g.,  $^{13}\text{C}/^{12}\text{C}$ ) because AGB stars and YSOs are known to have significantly different kinematics, especially

in a near-star region, and because  $^{13}\text{C}$  should be enhanced in a circumstellar envelope if the central star lies at the late-AGB stage.

#### 4. SUMMARY

In this Letter, we report results of an interferometric observation of an SiO maser source, IRAS 19312+1950, in the  $\text{HCO}^+ J = 1\text{--}0$  line. We found two kinematical components in the spectrum, a strong narrow line (narrow component) and a weak broad line (broad component). Velocity-integrated intensity maps show a pronounced bipolar shape consisting of the lower velocity part of the broad component. The higher velocity part of the broad component was not resolved by our synthesized beam and should originate in a relatively small region with a size of less than  $\sim 3''$ . The spatial structure of the narrow component clearly correlates with the near-infrared structure. In  $p$ - $v$  diagrams, a systematic variation of structure was found in the lower velocity part of the broad component, indicating the presence of a bipolar outflow. We suggest that the characteristics of the bipolar flow seen in IRAS 19312+1950 are explained by the interaction between an AGB wind and ambient material with axial symmetric structure.

The authors are grateful to Kee-Tae Kim, James R. Forster, Hiroshi Imai, and Hideyuki Izumiura for stimulating discussions and to Anthony Remijan for help with the BIMA observations and data reduction. We would also like to thank Douglas Friedel for his help in correcting our English and the anonymous referee for useful comments. This research has been supported by the Laboratory for Astronomical Imaging at the University of Illinois and by NSF grant AST 0228953 and has made use of the SIMBAD and ADS databases.

#### REFERENCES

- Balick, B., & Frank, A. 2002, *ARA&A*, 40, 439  
 Cox, P., Omont, A., Huggins, P., Bachiller, R., & Forveille, T. 1992, *A&A*, 266, 420  
 Deguchi, S., Izumiura, H., Kaifu, N., Mao, X., Nguyen-Q-Rieu, & Ukita, N. 1990, *ApJ*, 351, 522  
 Deguchi, S., & Nakashima, J. 2003, in *IAU Symp. 209, Planetary Nebulae: Their Evolution and Role in the Universe*, ed. S. Kwok, M. Dopita, & R. Sutherland (San Francisco: ASP), 259  
 Hasegawa, T., Morita, K., Okumura, S., Kaifu, N., Suzuki, H., Ohishi, M., Hayashi, M., & Ukita, N. 1986, in *Proc. Masers, Molecules and Mass Outflows in Star Forming Regions*, ed. A. D. Haschick (Westford: Haystack Obs.), 275  
 Kahane, C., & Jura, M. 1996, *A&A*, 310, 952  
 Kerschbaum, F., & Olofsson, H. 1999, *A&AS*, 138, 299  
 Knapp, G. R., Young, K., Lee, E., & Jorissen, A. 1998, *ApJS*, 117, 209  
 Mamon, G. A., Glassgold, A. E., & Omont, A. 1987, *ApJ*, 323, 306  
 Nakashima, J., & Deguchi, S. 2000, *PASJ*, 52, L43  
 ———. 2003a, *PASJ*, 55, 203  
 ———. 2003b, *PASJ*, 55, 229  
 Nakashima, J., Deguchi, S., & Kuno, N. 2004, *PASJ*, 56, 193  
 Nguyen-Q-Rieu, Deguchi, S., Izumiura, H., Kaifu, N., Ohishi, M., Suzuki, H., & Ukita, N. 1988, *ApJ*, 330, 374  
 Sánchez Contreras, C., Bujarrabal, V., Neri, R., & Alcolea, J. 2000, *A&A*, 357, 651  
 Sault, R. J., Teuben, P. J., & Wright, M. C. H. 1995, in *ASP Conf. Ser. 77, Astronomical Data Analysis Software and Systems IV*, ed., R. A. Shaw, H. E. Payne, & J. J. E. Hayes (San Francisco: ASP), 433  
 Welch, W. J., et al. 1996, *PASP*, 108, 93